Virus Research 274 (2019) 197771

Contents lists available at ScienceDirect

Virus Research

journal homepage: www.elsevier.com/locate/virusres

# Biodistribution of adeno-associated virus type 2 with mutations in the capsid that contribute to heparan sulfate proteoglycan binding

Oleg S. Gorbatyuk[a,b,c,2], Kenneth H. Warrington JR.[b,c,d,1], Marina S. Gorbatyuk[a,d,2], Irene Zolotukhin[b,c,d,1], Alfred S. Lewin[b,d], Nicholas Muzyczka[a,b,c,*]

[a] Department of Molecular Genetics and Microbiology, College of Medicine, University of Florida, United States
[b] Department of Pediatrics, College of Medicine, University of Florida, United States
[c] UF Genetics Institute, University of Florida, United States
[d] Powell Gene Therapy Center, College of Medicine, University of Florida, United States

ARTICLE INFO

*Keywords:*
Heparin mutant
Biodistribution
Virus gender bias
Virus retrograde transport
Liver transduction
Brain transduction
Eye transduction

ABSTRACT

We compared the phenotypes of three mutant AAV2 viruses containing mutations in arginine amino acids (R585, R588 and R484) previously shown to be involved in AAV2 heparan sulfate binding. The transduction efficiencies of wild type and mutant viruses were determined in the eye, the brain and peripheral organs following subretinal, striatal and intravenous injection, respectively, in mice and rats. We found that each of the three mutants (the single mutant R585A; the double mutant R585, 588A; and the triple mutant R585, 588, 484A) had a unique phenotype compared to wt and each other. R585A was completely defective for transducing peripheral organs via intravenous injection, suggesting that R585A may be useful for targeting peripheral organs by substitution of peptide ligands in the capsid surface. In the brain, all three mutants displayed widespread transduction, with the double mutant R585, 588A displaying the greatest spread and the greatest number of transduced neurons. The double mutant was also extremely efficient for retrograde transport, while the triple mutant was almost completely defective for retrograde transport. This suggested that R484 may be directly involved in interaction with the transport machinery. Finally, the double mutant also displayed improved transduction of the eye compared to wild type and the other mutants.

## 1. Introduction

Wild type AAV2 is the canonical dependovirus that has been characterized in detail at the genetic and biochemical level (Samulski and Muzyczka, 2014). Summerfeld and Samulski (Summerford and Samulski, 1998) demonstrated that it binds to heparan sulfate proteoglycans on the cell surface, and the current belief is that heparan sulfate is the primary ligand for cell attachment prior to cell entry. This is supported by the work of Kern et al. (Kern et al., 2003) and Opie et al. (Opie et al., 2003) who independently mapped the heparan binding residues on the virus surface and demonstrated that mutation of two of these amino acids, either R585 and R588, to alanine or glutamic acid reduced infectivity in cell culture up to a thousand-fold. They also identified 3 other amino acid residues that contributed to heparan binding: R484, R487 and K532. Subsequent work by Chen et al (Chen et al., 2005) demonstrated that native human isolates of AAV were predominantly AAV2, with 98% identity to the laboratory strain. All the native isolates had R585S and R588 T substitutions, suggesting that the arginine residues in the laboratory strain had been selected for their high infectivity in cell culture. A number of groups have examined the tropism of AAV2 mutants carrying substitutions in R585 and R588 to charged (E) or polar amino acids (S, T), and often these mutants contained other mutations as well (Boye et al., 2016; Kanaan et al., 2017; Tordo et al., 2018). This made it difficult to determine the effect of ablating heparin binding alone. In this report we compared the biodistribution and tissue tropism phenotypes of three heparin negative

* Corresponding author at: Department of Molecular Genetics and Microbiology, UF Genetics Institute and Powell Gene Therapy Center, College of Medicine, Cancer/Genetics Research Complex, 2033 Mowry Rd, Rm CG-208, Gainesville, FL, 32610, United States.
*E-mail addresses:* oleggor@uab.edu (O.S. Gorbatyuk), ken@lacertatherapeutics.com (K.H. Warrington), mgortk@uab.edu (M.S. Gorbatyuk), irene@lacertatherapeutics.com (I. Zolotukhin), lewin@mgm.ufl.edu (A.S. Lewin), nmuzyczk@ufl.edu (N. Muzyczka).
[1] Current address: Lacerta Therapeutics, 12085 Research Dr, Suite 46, Alachua, FL 32615.
[2] Current address: Department of Optometry and Vision Sciences, Center for Neurodegeneration and Experimental Therapy, University of Alabama at Birmingham, 1670 University Blvd, VH343, Birmingham, AL 35294-0019.

https://doi.org/10.1016/j.virusres.2019.197771
Received 10 June 2019; Received in revised form 25 September 2019; Accepted 27 September 2019
Available online 29 September 2019

mutants that we previously isolated containing the non-polar substitution A. They are the single mutation R585A, the double mutation R585, 588A, or the triple mutation R585, 588, 484A. Each was compared to the canonical wild type (wt) laboratory strain in mice and rats. We find that each of these mutants has a distinct phenotype in peripheral organs, as well as in the brain and the eye.

## 2. Materials and methods

### 2.1. Mutant construction and virus preparation

Construction of wt and mutant capsid plasmids was described previously (Opie et al., 2003). Transfection-quality plasmid DNA was produced by standard alkaline lysis method of a 1-liter culture followed by polyethylene glycol (PEG) precipitation and cesium chloride gradient purification. The AAV recombinant genome, pTRUF11, contains the coding sequence for humanized GFP under the control of the synthetic CBA promoter and the SV40 polyadenylation signal followed by the neomycin-resistance gene under the control of the mutant polyoma virus enhancer/promoter (PYF441) and the human bovine growth hormone poly(A) site, flanked by AAV2 TRs (Opie et al., 2003). Wt and mutant viruses was generated by three plasmid transfection into 293 cells using pIM45 (McCarty et al., 1991) containing wt and mutant capsid genes, pXX6 (Xiao et al., 1998) containing the Adenovirus helper genes and pTRUF11. Virus was purified by iodixanol step gradients and Sepharose Q column chromatography as previously described (Zolotukhin et al., 2002). All four virus stocks were at least 99% pure as judged by silver-stained SDS acrylamide gel fractionation. Vector titers were determined by dot-blot assay as described (Zolotukhin et al., 1999) and the titers were adjusted to $5 \times 10^{12}$ vector genomes (vg)/ml.

### 2.2. Biodistribution experiment

Ten mice (5 males and 5 females) were injected with $1.2 \times 10^{12}$ vector genomes of wt or one of the three mutants via tail vein. An additional 10 mice were injected with Lactated Ringers for a control. AAV genome copies using PCR were measured in accordance with University of Florida Powell Gene Therapy Center (PGTC) Toxicology Core SOP # TC-TL-008 – Real Time. Genomic DNA (gDNA) was isolated from blood and tissues using a DNeasy blood and tissue kit (Qiagen, Valencia, CA) according to the manufacturer's instructions and SOP # TC-TL-005 – Genomic DNA Extraction. gDNA concentrations were determined using the NanoDrop One system (Thermo Fisher) and SOP # TC-TL-018 – Genomic DNA Quantification. AAV genome copies present in gDNA were quantified by real-time PCR using the QuantStudio 3 Real-Time PCR System (Thermo Fisher, Carlsbad, CA) according to the manufacturer's instructions and SOP # TC-TL-008 – Real Time PCR, and results were analyzed using the QuantStudio Design & Analysis v1.4.1 software with the threshold, start baseline and stop baseline set automatically by the software. Briefly, primers and probe were designed to the SV40 polyadenylation region of the AAV vector used. A standard curve was performed using plasmid DNA containing the SV40 polyadenylation target sequence. PCR reactions contained a total volume of 50 µl and were run at the following conditions: 50 °C for 2 min, 95 °C for 10 min, and 45 cycles of 95 °C for 15 s and 60 °C for 1 min. DNA samples were assayed in triplicate. In order to assess PCR inhibition, the third replicate was spiked with plasmid DNA at a ratio of 100 copies/µg gDNA. If this replicate was greater than 40 copies/µg gDNA, then the results were considered acceptable. If a sample contained greater than or equal to 100 copies/µg gDNA, it was considered positive for vector genomes (vg). If a sample contained less than 100 copies/µg gDNA, it was considered negative for vector genomes. Vector copy numbers reported are normalized per µg gDNA. Assay controls include: a No Template Control (NTC) with acceptability criteria ≥40 cycle count (ct) and an established plasmid specific standard curve slope range (+/- 0.3 of the study mean slope determined from three individual standard preparations and runs). Data were reported as AAV genome copies per µg total genomic DNA.

### 2.3. Intracerebral injections of AAV vectors for microscopy and stereology

Eight female Sprague–Dawley rats were injected with each virus type into the striatum for histology and confocal imaging. Five animals were injected unilaterally, and three rats received injections in both sites of the brain with the same virus type. All surgical procedures were performed using aseptic conditions. The brain coordinates for the striatum were AP - 0.0 mm, Lat -3.0 mm, DV -4.0 mm. Injections were performed with a pulled glass micropipette with an outer diameter ~15-20 µm as previously (Burger et al., 2004). 2 µl of virus ($10^{10}$ vg) were injected at a rate of 0.5 µl/min. One min after the cessation of the injection the glass micropipette was retracted an additional 1 mm and then left in place for an additional 4 min before being slowly withdrawn from the brain.

### 2.4. Perfusion and tissue processing for histology

Four weeks after virus injections, animals were deeply anesthetized and perfused through the ascending aorta. Brains were perfused with 50 ml of isotonic saline, followed by 250 ml of ice-cold 4% paraformaldehyde in 0.1 M phosphate buffer (PB), pH 7.4. Brains were removed and post-fixed for 12 h in the same solution. The brains were then transferred to 30% sucrose in 0.1 M PB for cryoprotection. Forty-micrometer-thick coronal sections were cut on a freezing stage sliding microtome and processed for immunohistochemistry.

### 2.5. Immunohistochemistry

To identify colocalization of GFP with NeuN, GFAP, or TH, one series of sections from at least three animals per each viral vector were used. Sections were incubated sequentially in: (a) 1% donkey serum in PBS for 1 h; (b) one or an appropriate mixture of two primary antibodies, mouse monoclonal anti-NeuN (diluted 1:2000), mouse monoclonal anti-TH, and rabbit anti-GFAP (diluted 1:1000) (all antibodies obtained from Millipore, Billerica, MA, USA), which were diluted with 0.1% donkey serum and 0.3% Triton X-100 in PBS and incubated at room temperature for 24 h; and (c) one or a mixture of two secondary antibodies, Cy3-conjugated donkey anti-mouse IgG (diluted 1:100) and Cy5-conjugated donkey anti-rabbit IgG (diluted 1:100) (Jackson ImmunoResearch Laboratories, West Grove, PA, USA) in PBS for 2 h. The sections were rinsed in PBS for 30 min at room temperature between each incubation step. Mounted and coverslipped sections were examined with Leica laser scanning confocal microscope (Leica Microsystems CMS, Mannheim, Germany). To simplify interpretation of the results, artificial blue Cy5 color (GFAP) was replaced with red in Fig. 2 and, thus, the figure illustrates only GFP (green) and GFAP (red). All manipulations of contrast and illumination on color images as well as color replacement were made using Adobe PhotoShop software.

For the bright-field images (Fig. 5D) sections were preincubated first with 1% $H_2O_2$–10% methanol for 15 min and then with 5% normal goat serum for 1 h. Sections were incubated overnight at room temperature with anti-GFP antibody (Abcam at 1:2000 dilution). Incubation with secondary biotinylated anti-rabbit antibody was followed by incubation with avidin–biotin–peroxidase complex (ABC; Vector Laboratories, Burlingame, CA, USA). Reactions were visualized using 3,3-diaminobenzidine (DAB) as a chromagen.

### 2.6. Stereology

The unbiased stereological estimation of the total number of the GFP-positive neurons in each region was performed using the optical fractionator method as described previously (Burger et al., 2004). Sampling of cells to be counted was performed using the

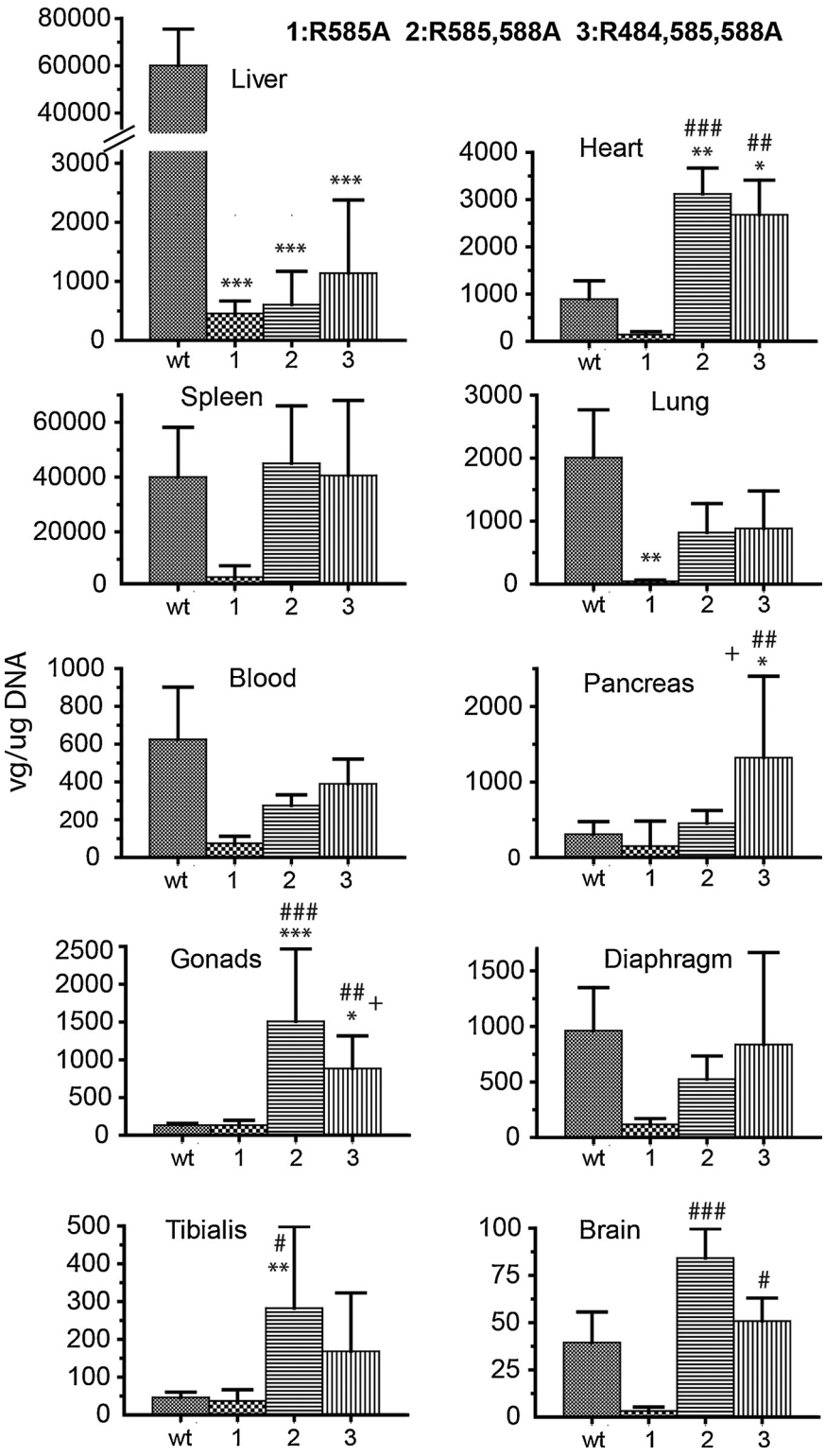


**Fig. 1. Viral genome copy numbers in selected tissues after mouse tail vein injection.** GFP genome copy numbers per μg of DNA in selected tissues at 4 weeks after tail vein injection of wild type (wt) and capsid mutant viral vectors. One-way ANOVA analysis was performed for each organ to compare wt and mutant injected animals. ANOVA statistics: liver $F[3,35] = 16.6$, $P < 0.0001$; spleen $F[3,34] = 1.79$, P = not significant (ns); blood $F[3,32] = 2.21$, P = ns; gonads $F[3,35] = 14.6$, $P < 0.0001$; tibialis anterior $F[3,31] = 5.77$, $P = 0.0033$; heart $F[3,34] = 8.2$, $P = 0.0003$; lung $F[3,36] = 4.09$, $P = 0.0135$; pancreas $F[3,32] = 5.55$, $P = 0.0035$; diaphragm $F[3,37] = 2.51$, P = ns; brain $F[3,34] = 6.34$, $P = 0.0016$. Tukey post hoc results are indicated as *, ** and *** = $P <$ 0.05, 0.01 and 0.001 respectively vs. wt AAV2; #, ## and ### = $P <$ 0.05, 0.01 and 0.001 respectively vs R585A; + = $P < 0.05$ vs R585, 588 A. N = 9–10 per group, except tibialis, which was 5–10 per group.

MicroBrightfield StereoInvestigator System. The software was used to delineate the transduction area at 4× objective and generate counting areas of 200× 200 μm. A counting frame was placed randomly on the first counting area and systematically moved through all counting areas until the entire delineated area was sampled. Actual counting was performed using a 40× objective. The estimate of the total number of neurons was calculated according to the optical fractionator formula (Burger et al., 2004; West et al., 1991). The coefficient of error due to the estimation was calculated according to Gundersen and Jenson (Gundersen and Jensen, 1987). Transduction volume was estimated using the Cavalieri method and was automatically calculated by the StereoInvestigator program.

### 2.7. Subretinal vector injection

C57Bl/6 mice were injected with wt and the mutant viruses at postnatal day 30. Animals (4 mice in each group) were anesthetized by intramuscular injection with mixture of ketamine and xylazine. The

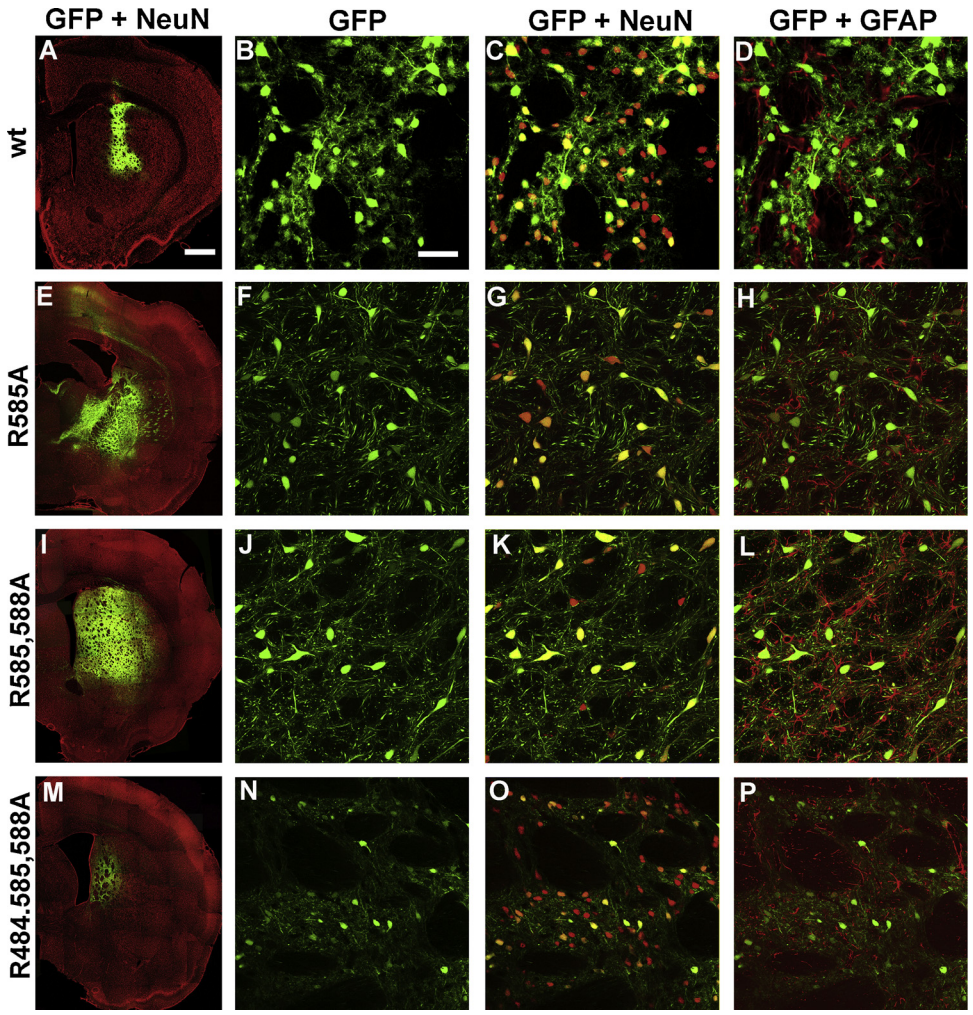


**Fig. 2. Confocal images of the rat striatum after injection of wild type rAAV2 (wt) or one of the mutant viral vectors.** (A, E, I, M) NeuN (red) and GFP (green) merged fluorescent images demonstrate the distribution area transduced with each viral vector in the striatum using approximately comparable slices. Gain in A was decreased 3–5 fold to match the fluorescence intensity in E, I, M (See Fig. 4 and text). (B–D, F–H, J–L, N–P) High magnification of the fluorescence images of the transduced areas in (A, E, I, M). Sections were visualized for native GFP (green) and immunostained for NeuN (Cy3-red) and GFAP (Cy5-blue was artificially substituted by red to simplify interpretation of the results). Images shown in (B, F, J, N) demonstrate GFP alone. Corresponding merge images show GFP and NeuN (C, G, K, and O) or GFP and GFAP (D, H, L and P). Note that few GFP-positive cells were also positive for GFAP, an astrocyte-specific marker. Scale bars: (A, E, I, M) 1 mm, (B–D, F–H, J–L, N–P) 50 μm.

concentration of viruses used for injection was $5 \times 10^{12}$ vg/ml. Animals received subretinal injections of 1 μl into right eye. Left eyes served as a control and were injected with saline buffer. All injections were administrated in accordance with the procedure described previously (Timmers et al., 2001).

### 2.8. Histological and immune-histological analysis

Eyes were fixed in 4% paraformaldehyde overnight at 4 °C. Eye cups were then transferred into phosphate buffered saline and submerged sequentially in solutions of 10%, 20% and 30% sucrose. Eye cups were then embedded in OCT medium (Sakura Finetek, Inc.) in order to produce 12 μm frozen sections. The frozen sections were used to visualize the level of viral transduction using confocal microscopy.

### 2.9. Evaluation of the level of viral transduction

Unbiased stereological counting was performed essentially as described above. GFP positive PR cells were counted in the ONL. Sections of mouse retina were stained with propidium iodide and sections of mouse retina fixed as described above were stained with propidium iodide. Images were taken on confocal fluorescent microscope for full retina mapping. Equal radial sections, starting from the optic nerve head (ONH), were used to count cells expressing GFP in the ONL. Comparison was performed by averaging 10 measurements of fluorescent cells in each sector.

### 2.10. Statistical analysis

One-way ANOVA with Tukey's post hoc analysis was performed using Graph Pad Prism software. Where indicated, two tailed t tests were performed.

## 3. Results

### 3.1. Biodistribution of mutants

As mentioned earlier, we and others have shown that R585 and R588 were primarily responsible for binding to heparan sulfate agarose *in vitro* and that three other basic residues R484, R487 and K532 also contributed to heparan binding (Kern et al., 2003; Opie et al., 2003). We, therefore, constructed the single substitution mutant R585A, the double substitution mutant R585A, R588A, and the triple substitution mutant, R585A, R588A, R484A. Both mutant and wild type viruses contained the GFP gene driven by the CMV-chicken β-actin enhancer-promoter (Opie et al., 2003). Virus was purified and titered by standard methods (See Methods) and injected via tail vein into 10 mice for wt virus and each of the three mutants at $1.2 \times 10^{12}$ vg/mouse. Equal numbers of both male and female mice were tested (n = 5 for both). An additional 10 mice were used as uninjected controls. Blood and organs were harvested 4 wks post injection and titered for the presence of GFP DNA by rtPCR with spike in controls as described in Methods.

We found that all three mutant viruses (R585A, R585, 588A and R484, 585, 588A) showed a significant decrease in transduction of liver compared to wt virus (0.8–1.6 % of wt) as determined by one-way

ANOVA analysis (Fig. 1). R585A was also significantly lower than wt for transducing the lung (Fig. 1). The difference between wt and the three mutants in transduction of spleen, diaphragm and blood did not reach statistical significance, although the single mutant R585A appeared to be the least active for transduction in all three organs (Fig. 1). Indeed, R585A produced the lowest transduction frequencies for all peripheral organs tested (Fig.1).

The double mutant R585, 588A was significantly higher for transduction of heart (3.5 fold), tibialis (6 fold) and gonads (11 fold) but not pancreas compared to wt. The triple mutant was significantly higher for transduction than wt in heart (4 fold), gonads (11 fold) and pancreas (4 fold) but not tibialis. Finally, brain produced the lowest transduction frequencies for both the mutants and wt. In general, the double mutant, R585, 588A, stood out as the best candidate for heart transduction.

### 3.2. Striatal brain injection

The striatum is a large brain structure, which we selected to investigate the extent of transduction of wt rAAV2 and capsid mutants, particularly because enervation of this region is affected in patients with Parkinson disease. We had previously shown that injection of wt rAAV2 into the rat striatum results in neuronal transduction of a very restricted area adjacent to the injection site (Burger et al., 2004). Therefore, we wanted to determine if mutation of the heparan sulfate glycosoaminoglycan (HSGAG) receptor binding motif significantly affects the extent of neuronal transduction. Female rats were injected unilaterally (N = 5) and bilaterally (N = 3) in the striatum ($1 \times 10^{10}$ vg in 2 µl per hemisphere) and brains were sectioned one-month post injection as described in Methods. Confocal microscopy analysis of brain sections showed that all three mutants transduced brain tissue to variable extents (Fig. 2 A, E, I, M). Immunocytochemistry with an antibody specific to the neuronal marker NeuN and an antibody against glial fibrillary acidic protein (GFAP), a marker for astrocytes, revealed that most if not all GFP expressing cells were also positive for NeuN for both wt and the three mutants (Fig. 2: B,C; F,G; J,K; N,O). In contrast, relatively few cells were positive for GFP and the astrocyte marker GFAP (B,D; F,H; J,L; N,P). This had previously been shown for wt AAV (Burger et al., 2004) and our results demonstrated that mutation of the heparan binding motif did not significantly change the neuronal tropism of AAV2. This has recently also been shown for the double mutant R585, 588A in mice (Sullivan et al., 2018).

To determine the extent to which virus transduction spread from the injection point, female rats were injected bilaterally (2 µl per side, N = 3) for each mutant and wt. Brains were then sectioned rostral to caudal and GFP expression was visualized by standard immunoperoxidase staining with antibody to GFP. We found that all three mutants produced a significantly greater spread of positive transduction compared to wt AAV2 from a single point injection, including the single mutant R585A that had been largely defective for transduction of peripheral organs (Fig. 3 A).

To determine the distribution area, rats were injected unilaterally with the mutants and wt (n = 5) and outlined areas containing GFP positive cells were counted with unbiased stereology on every $8^{th}$ serial 40µm-thick section (Fig. 3B, supplementary Fig. 1). As expected the size of the area ($\mu m^2$) containing GFP positive cells decreased with distance from the point of injection (Fig. 3B, supplementary Fig. 1). However, all three heparan mutants had a much broader dispersion than wt. R585A and the triple mutant R585, 588, 484A, spread to approximately the same extent (Fig. 3B and supplementary Fig. 1). The double mutant, however, appeared to spread over a significantly greater area (Fig. 3B, supplementary Fig. 1).

Stereology counting revealed that the improved spreading produced a significantly higher number of GFP-positive cells in animals injected with all three mutants compared to wt (Fig. 3C, *** $p < 0.001$ compared to wt). When we compared the three mutants against each other, R585, R588A injected animals had a significantly higher number of positive cells compared to both the R585A single mutant (Fig. 3C, # $p < 0.05$) and the R,585, 588, 484A triple mutant (Fig.3C, ## $p < 0.01$). Finally, there was no significant difference between the single mutant and the triple mutant. R585, 588A, on average, transduced 28-fold more cells than wt, and 40 and 60% more cells than the single and triple mutants, respectively.

We also calculated the transduction volume of wt and the three mutants. Consistent with the higher spread of virus, all three mutants displayed a significantly higher transduction volume than wt (Fig. 3D). The single, double and triple mutants had 5.4, 8.1- and 7.4-fold greater volumes than wt ($p < 0.001$) respectively, and the double mutant had a significantly greater volume (51%) than the single mutant (# $p < 0.05$). In contrast, when we calculated the number of GFP positive cells per unit volume, there was a trend toward lower numbers in the mutants compared to wt, but there was no significant difference between wt and mutants (Fig. 3E). For example, the double mutant R585, 588A, which transduced a 7.4-fold greater volume than wt (Fig. 3D), had only a 48% reduction in GFP positive cells per unit volume (Fig. 3E). Presumably, the increased volume of R585, 588A was not enough to dilute the number of input vg sufficiently to see a significant drop in vg/vol.

In principle, the confined space transduced by wt should produce much higher levels of expression in wt infected cells than mutant infected cells due to the high number of multiple hits per cell that occur near the site of injection. This was confirmed by comparing the intensity of GFP fluorescence at different levels of laser power using confocal microscopy (Fig. 4). The intensity of GFP fluorescence was much higher in wt infected cells than mutant infected cells at all laser intensities.

### 3.3. R585, 588A appears to be capable of efficient retrograde transport

To determine whether wt or mutant virus particles had the ability to be transported in the retrograde direction (i.e. from the synapse, toward the cell body), we analyzed brain sections from rats unilaterally injected in the right striatum. We examined GFP expression in areas that innervate the striatum, particularly the substantia nigra pars compacta (SNc). Brain sections were labeled with antibody for tyrosine hydroxylase (TH) to identify cell bodies of the SNc and examined by confocal microscopy (Fig. 5A–C). Animals injected with wt in the striatum showed only axons that were positive for GFP in the substantial nigra pars reticulata (SNr) (Fig. 5A). These axons presumably came from GFP positive cells in the striatum. In contrast animals injected with R585A or the double mutant R585, 588A showed a significant number of TH positive cells in the SNc that were also positive for GFP in their cell bodies. Since the spread of virus from the injection point did not extend to the SNc (Supplementary Fig. 1), this staining could only have occurred if viruses had entered SNc synapses or axons in the striatum and retrogradely transported to the cell bodies in the SNc, prior to expression. Moreover, the double mutant appeared to be capable of transducing virtually all the TH positive cells in SNc (compare Fig. 5C with the enlargement of the SNc region showing only green cells). Finally, the triple mutant showed only a handful of cells that had been successfully transduced via retrograde transport and it was necessary to use an antibody to GFP with immuperoxidase labeling to visualize single cells in the SNc (Fig. 5D).

Since the number of SNc neurons that terminate in the striatum are small compared to the total number of neurons in the striatum, it is possible that the improved retrograde transport of R585, 588A can be explained in part by the fact that the mutant virus is distributed in a significantly larger volume of the striatum than wt (Fig.3D), increasing the chance of contacting the membrane of axons passing through the striatal tissue from SNc. However, this clearly cannot be the only explanation, since the other two mutants show much lower or almost no retrograde transport despite having similar transduction frequencies and distribution in the striatum (Fig. 3 B,D). In addition, none of the

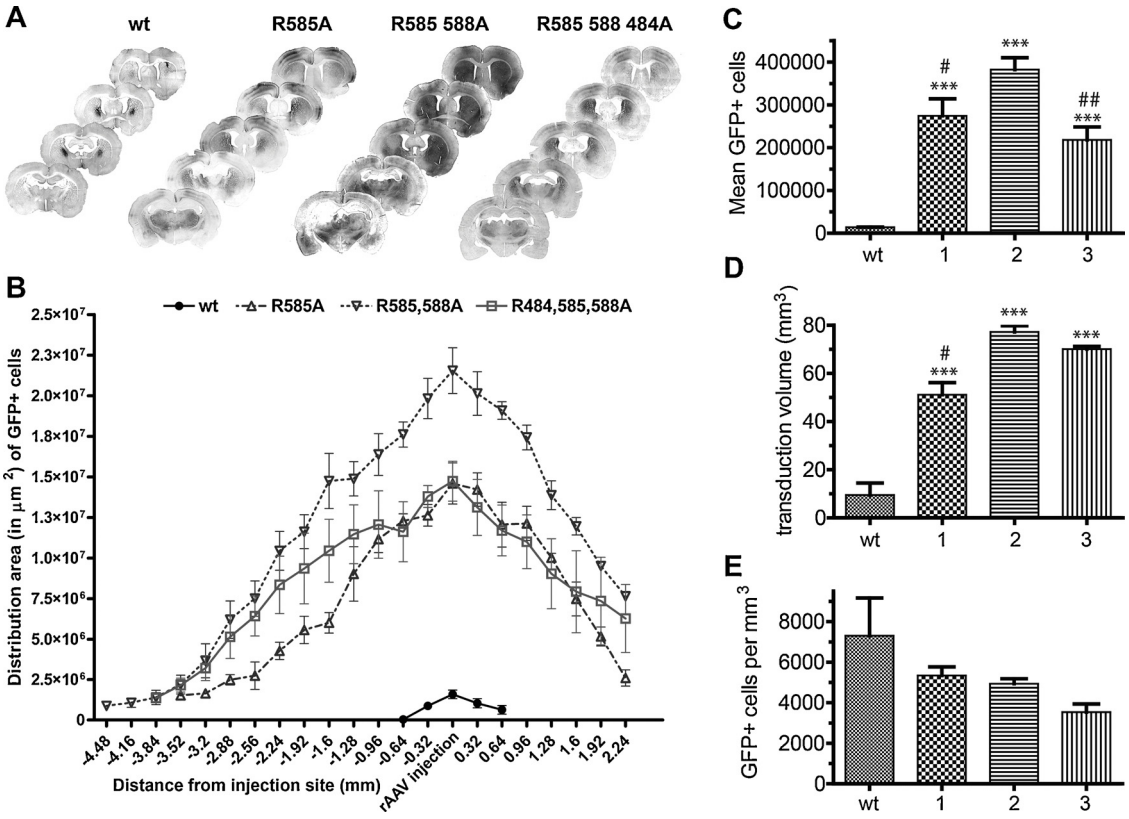


**Fig. 3.** Quantitative analysis of GFP-positive cells in the rat brain at 4 weeks after rAAV injections. (A) Montages of rostral-to-caudal coronal sections illustrate the extent of expression of GFP in the brain after bi-lateral injections with wt and mutant capsid viral vectors. These sections were visualized using standard immunoperoxidase labeling. (B) Rats were unilaterally injected with wt or mutant capsids. GFP-positive cells in every 8th serial section were delineated and demonstrate the comparative area of distribution (in $\mu m^2$) of each vector in each section. (C) The number of cells transduced with each viral vector were estimated from stereological counts in the serial sections shown in (B). (D) The total volume of distribution transduced with wt or mutant capsids was calculated from the serial sections shown in (B). (E) The number of transduced cells per volume ($mm^3$) calculated from measurements shown in (C and D). One-way ANOVA for panel C: F[3,15] = 50.62, P < 0.0001; for panel D: F[3,15] = 44.76, P < 0.0001; for panel E: F[3,16] = 1.13, P = 0.36. Tukey post hoc results are indicated as *** = P < 0.001 vs. wt AAV2; # and ## = P < 0.05 and 0.01 respectively vs R585, 588A. N = 4 for mutants and 8 for wt in panels B, C, D and E. Only female rats were used for these experiments.

viruses demonstrated a diffusion that extended to the SNc from the injection site (Supplementary Fig. 1).

### 3.4. Subretinal injection

We also compared the transduction efficiency of wt and mutant viruses in the mouse eye. Sub-retinal injection of wt and mutant viruses into C57Bl/6 mice demonstrated that GFP expression was found in photoreceptors cells (PR) of the outer nuclear layer (ONL) and outer segments (OS) (Supplementary Fig. 2, top). In addition, in all injected retinas expression of GFP was observed in retinal pigment epithelium (RPE). We also found that transduction by wt; R585A, R585; 588A and, R585, 588, 484A, was not limited by the site of injection in the subretinal space and extended across the full retina Supplementary Fig. 2: top, A, D, G, J). However, it is necessary to mention that the density of viral transduction was not equal in all injected retinas (compare Supplementary Fig. 2, top: C, F, L).

Stereological counting of GFP expressing PR cells was performed in the ONL and calculated as the number of GFP-positive cells per 1000 propidium iodide labeled cells in the ONL (Supplementary Fig. 2, bottom). The number of transduced PR cells in retinas injected with wt, R585A, and, R585, 588, 484A was not significantly different (121 ± 15, 127 ± 17 and 101 ± 14, respectively). The only exception found was the double mutant R585, 588A, which transduced a significantly higher number of PR cells, approximately a two-fold difference compared to the other viruses, 232 ± 22 cells or an efficiency of transduction of 23% (Supplementary Fig. 2 bottom: $p <$ 0.01 compared to wt and R585A and $p < 0.001$ compared to R585, 588, 484A).

## 4. Discussion

### 4.1. Each mutant had a unique phenotype in peripheral organs

Wild type AAV2 transduced liver at a higher level than any other organ, but all three mutants essentially eliminated liver transduction (Fig. 1). This confirmed previous observations by Kern et al (Kern et al., 2003) who examined the R487, 585E mutant and by Perabo et al (Perabo et al., 2006), who tested the effect of small oligopeptide insertions at aa 587 that also abolished heparan binding. Boye et al (Boye et al., 2016) tested the substitution of R585, R588 and R487 with the native amino acids S, T and G respectively, in the presence of 4 other mutations (AAV2 (4pMut)ΔHS): Y444 F, Y500 F, Y730 F, T481 V. They showed that this 7 amino acid mutant also did not infect liver using *in vivo* imaging when compared to the heparan positive control. Finally, Sullivan et al (Sullivan et al., 2018) tested the R585, R588A double mutant via intravenous injections. Like us, they saw almost a complete elimination of liver transduction. Unlike the previous studies, our study demonstrated that mutation of R585 alone was sufficient to completely eliminate liver transduction. Taken together, these observations suggest that heparan binding alone is the primary determinant for liver transduction.

The spleen was transduced almost as well as liver by wt AAV but, except for R585A, the mutants showed transduction of spleen that was

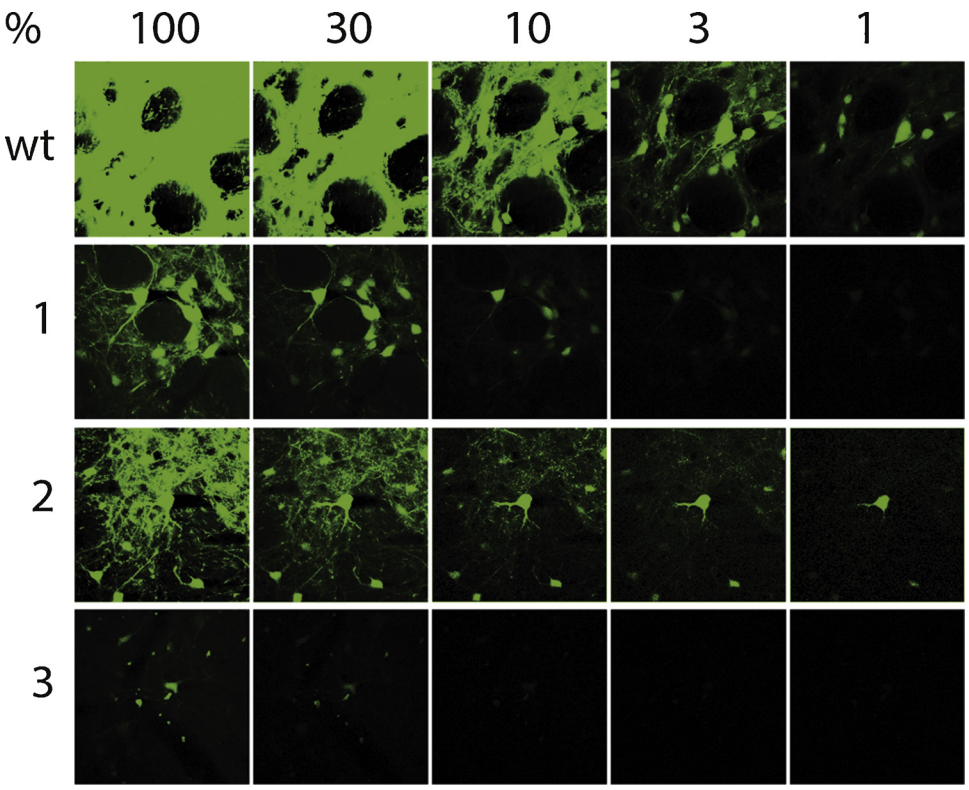


**Fig. 4. Confocal images illustrate intensity level of GFP fluorescence produced by wt and capsid mutants in rat striatum**. Striatal sections taken near the site of injection were photographed by confocal microscopy. The same setting was used for all virus types as the level of laser power was gradually reduced (100%, 30%, 10%, 3% and 1%).

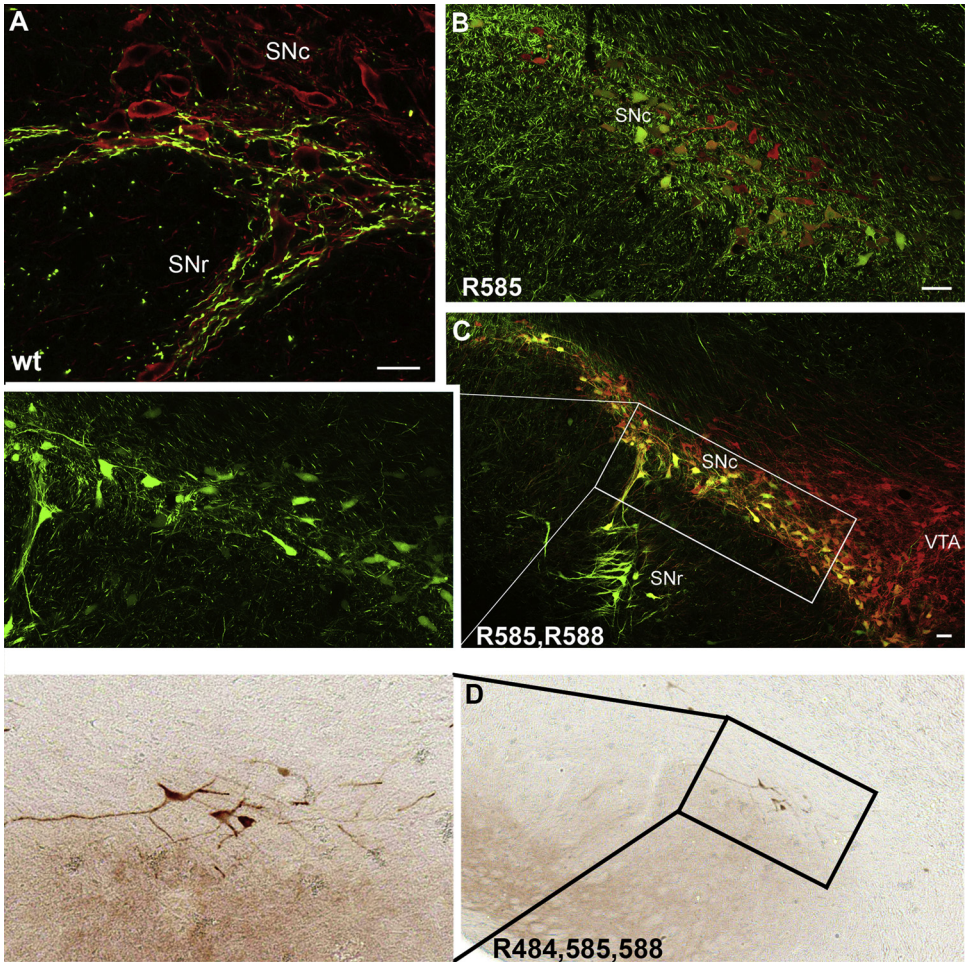


**Fig. 5. Retrograde transport of wt rAAV and mutants in rat brain.** Merged views showing TH-positive rat neurons (red) that had been injected with GFP-expressing wt and mutants following unilateral injection in the striatum. (A) GFP tracing of the anterograde axonal projections to the substantia nigra pars reticulata (SNr) following injection of wt vector. There were no GFP expressing TH-positive cell bodies in the substantia nigra pars compacta (SNc). (B) Some cell bodies of the SNc were positive for GFP following retrograde transport of the R585A mutant from a striatal injection on same side. (C) Confocal image demonstrating widespread, selective transduction of dopaminergic neurons in the SNc after R585, 588A mutant injection into the striatum. Enlarged boxed area shown with only green cells. (D) Only single GFP expressing nigral neurons were detected with standard immune-peroxidase method in rats injected with R484, 585, 588A mutant virus. Notably, there were no TH-positive cells in the ventral tegmental area (VTA) expressing GFP or GFP –positive cells in any surrounding structures. All scale bars: 50 μm.

comparable to wt. R585A was unique in that there was a major loss in transduction in all peripheral organs tested. Given R585A's robust transduction of eye and brain, this was not likely to be due to some defect specific to the R585A virus preparation. Our data thus suggest that mutation of R585 reduces infection of all peripheral organs, and this would make it an excellent backbone for introduction of targeting ligands.

Heart was the third most efficiently transduced organ, but in this case, the most efficient transduction was achieved by the double and triple mutants, which showed a significant increase in heart compared to wt. Higher transduction of heart compared to wt was similar to what was reported previously for the R484, R585E double mutant (Kern et al., 2003; Muller et al., 2006) and the R585, R588A double mutant (Sullivan et al., 2018). All three studies suggest that heparan independent transduction of heart uses either a different entry process or a different post entry mechanism compared to liver. Our results also suggest that eliminating heparan binding alone, as with the R585A mutant, is not sufficient for targeting the heart. The data suggest that R585, 588A may be a good candidate for gene transfer to the heart via the intravascular route.

### 4.2. Heparan mutants show robust transduction of brain

All three heparan negative mutants showed robust transduction of striatum from a point injection in brain parenchyma (Figs. 2 and 3). The double mutant, R585, 588A, generated the greatest spread (Fig. 3A,B,D, supplementary Fig. 1) and the highest number of transduced cells (Fig. 3C). The fact that the single mutant and triple mutant were significantly lower for transduction (Fig. 3C) and spread suggests that eliminating heparan binding alone was not the only mechanism by which R585, 588A was more efficient for virus spread or increased transduction. Either the double mutant was more efficient at entering cells or, as discussed below, it was more capable of undergoing retrograde transport.

As expected, the intensity of GFP expression increased as the volume of transduction decreased so that cells infected with wt, which received more genome copies per cell, displayed much higher GFP fluorescence per cells (Fig. 4). However, it is worth noting that there was no significant difference between wt and the mutants in the number of GFP positive cells per volume of transduction (Fig. 3E). This suggested that despite the higher volume of transduction displayed by R585, 588A and the other mutants, there was still a considerable number of genomes that were essentially wasted through multiple hits of the same cells. We calculated that the injection of $10^{10}$ vg of the double mutant transduced $3.8 \times 10^5$ neurons for an apparent transduction efficiency (particle to infectivity ratio) from a point injection of approximately 26,000 vg/transduced cell. This transduction efficiency is likely to become much better if an alternative, more efficient method of introducing vector into the CNS is used, for example, intrathecal injection, in which the spread of vector may be even higher.

We note that Kanaan and colleagues (Kanaan et al., 2017) tested a different triple heparan negative mutant containing the native R585S, R588 T, R487 G heparan substitutions and the additional mutations Y444, 500, 730 F and T491 V. Following striatal injections at virus loads approximately 4-fold lower than used in our study and the same volumes, this group saw approximately a 23% increase in GFP positive cells compared to the heparin positive control in a volume of approximately 22 $mm^3$. In contrast, the triple mutant R585A, R588A, R484A reported here increased the number of heparan positive cells compared to wt by 16-fold in a volume of 71 $mm^3$. Taken together, the two studies suggest that the additional Y and T substitutions or the different heparan substitutions in the Kanaan et al study may have modulated the heparan effect or that transduction is not a simple linear function of input virus. Tordo et al (Tordo et al., 2018) tested an AAV2 derived virus (AAV-TT) that contained the 14 amino acid substitutions that were found in the native virus found in pediatric patients by Chen and co-workers (Chen et al., 2005). The mutant had R585S and R588 T mutations like those of Kanaan et al. (Kanaan et al., 2017) but a different set of additional substitutions (N321S, Q451 M, S492A, E499D, F533Y, G546D, E548 G, A593S). Injection of $3.5 \times 10^9$ vg into rat striatum produced transduction profiles similar to those seen in our study, but as in the Kanaan et al. study, it was not clear which mutations contributed to the increased transduction frequency. Finally, Sullivan and colleagues (Sullivan et al., 2018) and Naidoo et al. (Naidoo et al., 2018) performed intrastriatal mouse injections or intracerebroventricular and intrathalamic injections of non-human primates, respectively, using the R585,588A double mutant. As seen in this study, they found robust transduction of brain tissue.

### 4.3. Retrograde transport

R585, 588A was unique among the mutants in its ability to efficiently undergo retrograde transport (Fig. 5). This feature was shared to a limited extent by the single mutant R585A. Both mutants are gain of function mutants suggesting that the arg residues inhibit attachment to the transport machinery either due to their charge or their bulky size. The triple mutant (R585, 588, 484A) on the other hand, showed almost a complete loss of retrograde transport suggesting that R484 is likely to be involved directly in virus binding to the transport machinery. All three residues are situated near the highest point of the virus surface (Xie et al., 2002). Examination of the position of the three residues in the virus structure (Fig. 6) shows that R585 and R588 partially occlude R484, which lies beneath them. This is consistent with the idea that conversion of R585 and R588 to alanine, a small non-polar amino acid, allows access to R484 by the transport machinery. The fact that R585, 588A and R585A can undergo efficient retrograde transport makes them potentially useful for transduction of brain cells via intravenous injection. R585, 588A has also been shown to undergo retrograde transport in non-human primates (Naidoo et al., 2018).

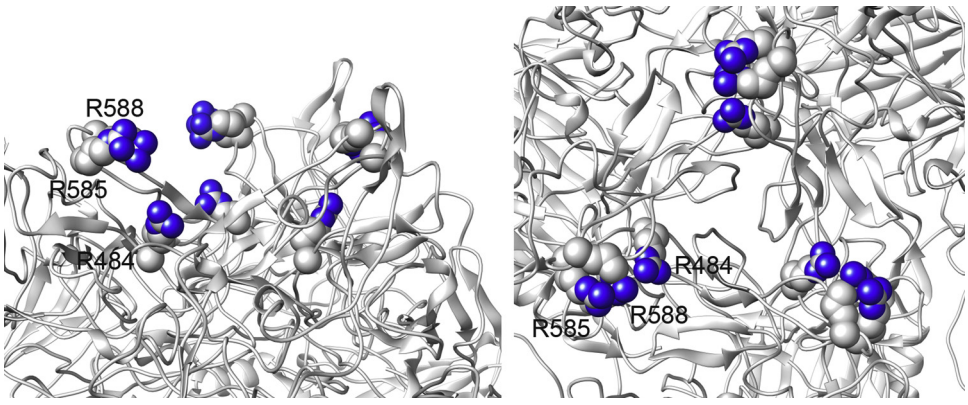


**Fig. 6. Left panel:** Approximately 60° side view of the capsid trimer interface showing the positions of the three residues, R585, R588 and R484, that were mutated. The three capsid proteins forming the trimer interface are shown as ribbon traces and the atoms of the 3 residues are shown as spheres; gray spheres are carbon atoms and blue spheres are nitrogen. **Right panel:** A top down view of the three-fold interface showing the positions of the three residues. Note that R585 and R588 partially occlude R484.

### 4.4. Eye transduction

Finally, R585,588A was unique in that it was significantly better than wt and the other mutants in transducing photoreceptor cells of the eye following subretinal injection (Supplementary Fig. 2). However, the increase in transduction was a relatively modest 2-fold. In contrast when Boye et al (Boye et al., 2016) tested their heparan negative mutant (AAV2(4pMut)ΔHS) carrying the native substitutions R585S, R588 T R487 G as well as 4 other mutations (Y444, 500,730 F, T491 V) they found up to a 7-fold increase in photoreceptor transduction compared to the heparan positive control. This may be due to synergy with the non-heparan mutations or due to the different mouse line that was used in the two studies (Nrl-GFP vs C57B/L6).

### 4.5. Conclusion

Our study demonstrates that mutation of R585 alone eliminates transduction of liver and all other peripheral organs in mice. Thus, R585A may be ideal for targeting specific organs in the periphery via attachment of oligopeptide ligands. Our work also suggests that the relatively simple heparan negative double mutant, R585A, R588A, may be useful for global distribution of AAV vector in the brain. Alternative injection strategies such as intrathecal or intraventricular, when used in combination with R585, 588A may produce the kind of widespread transduction that is necessary for effective treatment of neurodegenerative or lysosomal diseases. In addition, our study suggests that R585, 588A appears to be capable of efficient retrograde transport and that residue R484 may be directly involved in interacting with the retrograde transport machinery. Finally, there does not seem to be a major advantage to using the double mutant for subretinal gene transfer to the eye.

NM is a founder and stock holder of Applied Genetic Technologies Corp. (AGTC) and a founder and stock holder of Lacerta Therapeutics, Inc. NM is also an inventor on several AAV patents. KHW is a founder of Lacerta Therapeutics and an inventor on an AAV patent. IZ and KHW are employees of Lacerta Therapeutics. AGTC and Lacerta Therapeutics are developing gene therapy applications for the eye and brain, respectively, using AAV vectors.

## Declaration of Competing Interest

NM is a founder and stock holder of Applied Genetic Technologies Corp. (AGTC) and a founder and stock holder of Lacerta Therapeutics, Inc. NM is also an inventor on several AAV patents. KHW is a founder of Lacerta Therapeutics and an inventor on an AAV patent. IZ and KHW are employees of Lacerta Therapeutics. AGTC and Lacerta Therapeutics are developing gene therapy applications for the eye and brain, respectively, using AAV vectors.

## Acknowledgements

The authors thank Wei-jun Chen and Craig Meyer for technical assistance. Biodistribution experiments were carried out by the Toxicology Core of the Powell Gene Therapy Center at the University of Florida. This work was supported by grants from NIH-NHLBI PO1HL59412 and PO1HL51811, NIH-NINDS PO1NS36302 and RO1NS64268, NIH-GM GM109524, and the ACS Edwin R. Koger Endowed chair.

## Appendix A. Supplementary data

Supplementary material related to this article can be found, in the online version, at doi:https://doi.org/10.1016/j.virusres.2019.197771.

## References

Boye, S.L., Bennett, A., Scalabrino, M.L., McCullough, K.T., Van Vliet, K., Choudhury, S., Ruan, Q., Peterson, J., Agbandje-McKenna, M., Boye, S.E., 2016. Impact of heparan sulfate binding on transduction of retina by recombinant adeno-associated virus vectors. J. Virol. 90 (8), 4215–4231.

Burger, C., Gorbakyuk, O., Velardo, M.J., Peden, C., Williams, P., Zolotukhin, S., Reier, P.J., Mandel, R.J., Muzyczka, N., 2004. Recombinant AAV viral vectors pseudotyped with viral capsids from serotypes 1, 2, and 5 display differential efficiency and cell tropism after delivery to different regions of the central nervous system. Mol. Ther. 10 (2), 302–317.

Chen, C.L., Jensen, R.L., Schnepp, B.C., Connell, M.J., Shell, R., Sferra, T.J., Bartlett, J.S., Clark, K.R., Johnson, P.R., 2005. Molecular characterization of adeno-associated viruses infecting children. J. Virol. 79 (23), 14781–14792.

Gundersen, H.J., Jensen, E.B., 1987. The efficiency of systematic sampling in stereology and its prediction. J. Microsc. 147 (Pt 3), 229–263.

Kanaan, N.M., Sellnow, R.C., Boye, S.L., Coberly, B., Bennett, A., Agbandje-McKenna, M., Sortwell, C.E., Hauswirth, W.W., Boye, S.E., Manfredsson, F.P., 2017. Rationally engineered AAV capsids improve transduction and volumetric spread in the CNS. Mol. Ther. Nucleic Acids 8, 184–197.

Kern, A., Schmidt, K., Leder, C., Muller, O.J., Wobus, C.E., Bettinger, K., Von der Lieth, C.W., King, J.A., Kleinschmidt, J.A., 2003. Identification of a heparin-binding motif on adeno-associated virus type 2 capsids. J. Virol. 77 (20), 11072–11081.

McCarty, D.M., Christensen, M., Muzyczka, N., 1991. Sequences required for coordinate induction of adeno-associated virus p19 and p40 promoters by Rep protein. J. Virol. 65, 2936–2945.

Muller, O.J., Leuchs, B., Pleger, S.T., Grimm, D., Franz, W.M., Katus, H.A., Kleinschmidt, J.A., 2006. Improved cardiac gene transfer by transcriptional and transductional targeting of adeno-associated viral vectors. Cardiovasc. Res. 70 (1), 70–78.

Naidoo, J., Stanek, L.M., Ohno, K., Trewman, S., Samaranch, L., Hadaczek, P., O'Riordan, C., Sullivan, J., San Sebastian, W., Bringas, J.R., Snieckus, C., Mahmoodi, A., Forsayeth, J., Bankiewicz, K.S., Shihabuddin, L.S., 2018. Extensive transduction and enhanced spread of a modified AAV2 capsid in the non-human primate CNS. Mol. Ther. 26 (10), 2418–2430.

Opie, S.R., Warrington Jr Jr., K.H., Agbandje-McKenna, M., Zolotukhin, S., Muzyczka, N., 2003. Identification of amino acid residues in the capsid proteins of adeno-associated virus type 2 that contribute to heparan sulfate proteoglycan binding. J. Virol. 77 (12), 6995–7006.

Perabo, L., Goldnau, D., White, K., Endell, J., Boucas, J., Humme, S., Work, L.M., Janicki, H., Hallek, M., Baker, A.H., Buning, H., 2006. Heparan sulfate proteoglycan binding properties of adeno-associated virus retargeting mutants and consequences for their in vivo tropism. J. Virol. 80 (14), 7265–7269.

Samulski, R.J., Muzyczka, N., 2014. AAV-mediated gene therapy for research and therapeutic purposes. Annu. Rev. Virol. 1 (1), 427–451.

Sullivan, J.A., Stanek, L.M., Lukason, M.J., Bu, J., Osmond, S.R., Barry, E.A., O'Riordan, C.R., Shihabuddin, L.S., Cheng, S.H., Scaria, A., 2018. Rationally designed AAV2 and AAVrh8R capsids provide improved transduction in the retina and brain. Gene Ther. 25 (3), 205–219.

Summerford, C., Samulski, R.J., 1998. Membrane-associated heparan sulfate proteoglycan is a receptor for adeno-associated virus type 2 virions. J. Virol. 72 (2), 1438–1445.

Timmers, A.M., Zhang, H., Squitieri, A., Gonzalez-Pola, C., 2001. Subretinal injections in rodent eyes: effects on electrophysiology and histology of rat retina. Mol. Vis. 7, 131–137.

Tordo, J., O'Leary, C., Antunes, A., Palomar, N., Aldrin-Kirk, P., Basche, M., Bennett, A., D'Souza, Z., Gleitz, H., Godwin, A., Holley, R.J., Parker, H., Liao, A.Y., Rouse, P., Youshani, A.S., Dridi, L., Martins, C., Levade, T., Stacey, K.B., Davis, D.M., Dyer, A., Clement, N., Bjorklund, T., Ali, R.R., Agbandje-McKenna, M., Rahim, A.A., Pshezhetsky, A., Waddington, S.N., Linden, R.M., Bigger, B.W., Henckaerts, E., 2018. A novel adeno-associated virus capsid with enhanced neurotropism corrects a lysosomal transmembrane enzyme deficiency. Brain 141 (7), 2014–2031.

West, M.J., Slomianka, L., Gundersen, H.J., 1991. Unbiased stereological estimation of the total number of neurons in the subdivisions of the rat hippocampus using the optical fractionator. Anat. Rec. 231 (4), 482–497.

Xiao, X., Li, J., Samulski, R.J., 1998. Production of high-titer recombinant adeno-associated virus vectors in the absence of helper adenovirus. J. Virol. 72 (3), 2224–2232.

Xie, Q., Bu, W., Bhatia, S., Hare, J., Somasundaram, T., Azzi, A., Chapman, M.S., 2002. The atomic structure of adeno-associated virus (AAV-2), a vector for human gene therapy. Proc. Natl. Acad. Sci. U. S. A. 99 (16), 10405–10410.

Zolotukhin, S., Byrne, B.J., Mason, E., Zolotukhin, I., Potter, M., Chesnut, K., Summerford, C., Samulski, R.J., Muzyczka, N., 1999. Recombinant adeno-associated virus purification using novel methods improves infectious titer and yield. Gene Ther. 6 (6), 973–985.

Zolotukhin, S., Potter, M., Zolotukhin, I., Sakai, Y., Loiler, S., Fraites Jr., T.J., Chiodo, V.A., Phillipsberg, T., Muzyczka, N., Hauswirth, W.W., Flotte, T.R., Byrne, B.J., Snyder, R.O., 2002. Production and purification of serotype 1, 2, and 5 recombinant adeno-associated viral vectors. Methods 28 (2), 158–167.